Research Article | Vol. 40, No. 6 / June 2023 / Journal of the Optical Society of America A 1225

OPTICS, IMAGE SCIENCE, AND VISION

Considerations for excess noise measurements of low-*k*-factor Sb-based avalanche photodiodes

ADAM A. DADEY,[1] J. ANDREW MCARTHUR,[2] ANDREW H. JONES,[1] SETH R. BANK,[2] AND JOE C. CAMPBELL[1,*]

[1]Department of Electrical and Computer Engineering, University of Virginia, Charlottesville, Virginia 22903, USA
[2]Department of Electrical and Computer Engineering, University of Texas at Austin, Austin, Texas 78758, USA
*jcc7s@virginia.edu

Received 21 April 2023; accepted 4 May 2023; posted 9 May 2023; published 31 May 2023

In applications where high sensitivity is required, the internal gain mechanism of avalanche photodiodes can provide a performance advantage relative to p-i-n photodiodes. However, this internal gain mechanism leads to an excess noise that scales with gain. This excess noise term can be minimized by using materials systems in which impact ionization is initiated primarily by one carrier type. Recently, two Sb-based materials systems, AlInAsSb and AlGaAsSb, have exhibited exceptionally low excess noise, particularly for III–V compound materials. There are four important considerations that can impact the excess noise measurements in such low-noise materials. These considerations deal with the excess noise factor calculation method, measurement RF frequency, measurement wavelength, and the gain calculation method. In this paper, each of these factors is discussed, and their implications on excess noise are considered. © 2023 Optica Publishing Group

https://doi.org/10.1364/JOSAA.493819

1. INTRODUCTION

For applications where high sensitivity is required an avalanche photodiode (APD) can provide a distinct advantage over a simple p-i-n photodiode owing to its internal gain mechanism created by impact ionization. As a result, APDs have been widely deployed in a wide range of applications including high-speed optical communications, lidar, imaging, and single-photon detection [1]. However, impact ionization is a stochastic process resulting in a shot-noise power described by

$$N_{\mathrm{APD}} = 2q(I_{\mathrm{photo}} + I_{\mathrm{dark}})R\Delta f M^2 F(M), \quad (1)$$

where q is the elementary charge, I_{photo} and I_{dark} are the photocurrent and dark current, respectively, R is the system impedance, Δf is the system bandwidth, M is the gain, and $F(M)$ is the excess noise factor. The excess noise factor in an APD is frequently expressed using the local field model [2],

$$F(M) = kM + (1-k)(2-1/M), \quad (2)$$

where k is defined as the ratio among β, the hole impact ionization coefficient, and α, the electron impact ionization coefficient. For the lowest impact on APD noise, a k factor of zero gives an excess noise factor that approaches 2 at high gain. Silicon is a well-known material with a near-zero k factor of ∼0.01 [3]. Recently two Sb-based material systems have emerged, $Al_xIn_{1-x}As_ySb_{1-y}$ (hereafter Al_xInAsSb) grown on GaSb [4–7], InP [8], and $Al_xGa_{1-x}As_ySb_{1-y}$ (hereafter Al_xGaAsSb) grown on InP [9–11], both of which have exhibited near-zero k factors on the order of 0.01–0.05.

When measuring the excess noise of an APD, especially those with low-k factors, there are several factors to consider regarding the proper measurement and calculation of $F(M)$. Specifically, this paper presents four considerations that affect the resulting $F(M)$. The first consideration compares the calculation of $F(M)$ using a single reference point versus a calculation based on a reference line. Second, three measurement setups are presented for performing measurements at different operating frequencies. Third, the wavelength dependence of $F(M)$ is considered. Finally, two different gain correction methods are presented to compensate for bias-dependent responsivity in the APD structure. Each of these four considerations is explained in the subsequent sections.

2. DEVICE GROWTH AND FABRICATION

To perform this study, $Al_{0.7}$InAsSb epitaxial layers were grown as a digital alloy on an n-type GaSb substrate via molecular-beam epitaxy as described in a previous publication [12]. Figure 1 shows a schematic cross section of the device. Circular mesas were defined using standard lithography techniques. Mesas were formed using a $C_6H_8O_7$:H_3PO_4:H_2O_2:H_2O (10 g:6 ml:3 ml:60 ml) wet etch. Ti/Au (10 nm/100 nm) contacts were deposited for both the p- and n-contact layers. Finally, the mesa sidewalls were passivated with SU-8 to reduce the surface leakage current.

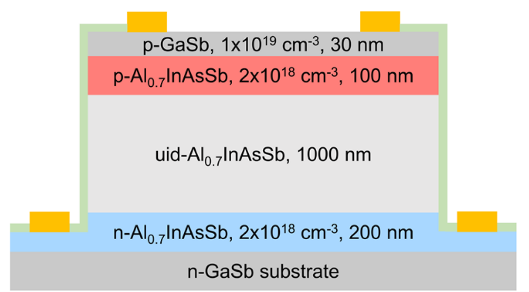

Fig. 1. Schematic cross section of the $Al_{0.7}InAsSb$ p-i-n APD structure used in this paper.

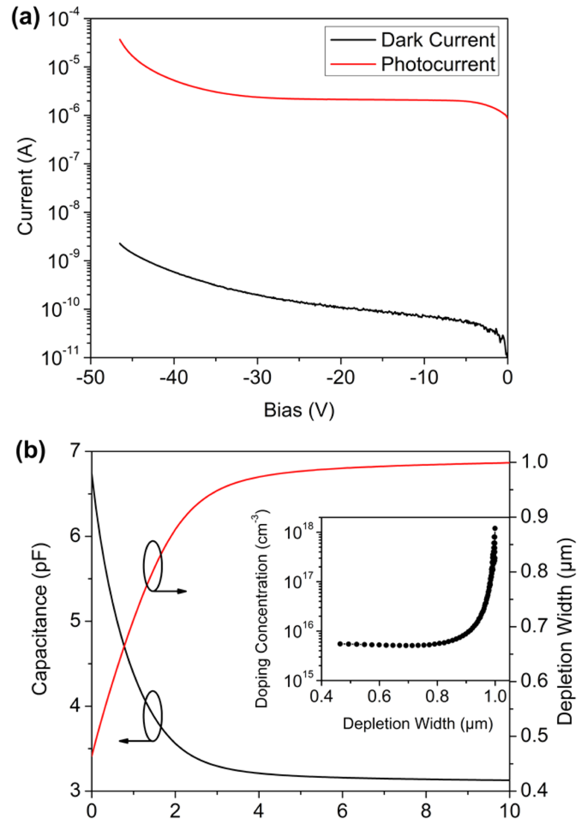

Fig. 2. (a) C-V curves under blackout conditions and ∼46 μW of 543 nm illumination for a 100 μm diameter device. (b) C-V curve (black) and depletion width versus voltage curve (red) for a 200 μm diameter device under blackout conditions, and (inset) the doping concentration versus depletion width calculated from the C-V curve.

3. CURRENT-VOLTAGE AND CAPACITANCE-VOLTAGE CHARACTERISTICS

Current-voltage (I-V) measurements were performed with a Keithley 2400 SourceMeter. Figure 2(a) shows the dark current, measured under blackout conditions, and photocurrent, under ∼46 μW of 543-nm He–Ne laser illumination for a 100 μm diameter device.

Capacitance-voltage (C-V) measurements were performed with a HP 3275A LCR meter at 1 MHz under blackout conditions. Figure 2(b) shows a C-V curve and a depletion width versus the voltage curve for a 200 μm diameter device. The depletion width was calculated assuming a parallel plate capacitor model where a relative permittivity of 13.9 was used. The inset of Fig. 2(b) shows the calculated doping concentration versus the depletion width extracted from the measured C-V, using a method detailed in a previous publication [13]. As shown in the inset, the unintentional doping (uid) concentration in the "intrinsic" region is $\sim 5 \times 10^{15}$ cm^{-3}.

4. $F(M)$ CALCULATION: SINGLE POINT VERSUS PHOTOCURRENT-DEPENDENT REFERENCE LINE

Unless otherwise noted, all excess noise measurements in this paper were performed with an Agilent 8973 noise figure analyzer (NFA) at 50 MHz with a 4 MHz bandwidth under 543 nm He–Ne laser illumination on 100 μm diameter devices.

Normally, the excess noise of an APD can be measured by taking a fixed light intensity and varying the bias to achieve increased gain. At each bias point, the noise is measured without illumination and is subtracted from the noise measured under illumination. Such a measurement results in a curve such as the red points in Fig. 3(a). If the first bias point is at a sufficiently low bias such that there is no gain ($M = 1$) and $F(M) = 1$, that point can be used as a reference. Neglecting dark current, this first point (N_{unity}) represents the terms $2q I_{photo} R\Delta f$ from (1). The gain is determined by increasing the bias and taking the ratio of the photocurrent to that of the unity gain point. $F(M)$ can then be calculated using the following expression:

$$F(M) = N_{measured}/(N_{unity} M^2), \tag{3}$$

where $N_{measured} = 2q I_{photo} R\Delta f M^2 F(M)$ is the measured noise under higher bias with gain, M and, N_{unity} is the noise of the first unity gain point. This method works if there is little error in the measurement of the first point. However, since every subsequent measured bias point relies on the accuracy of the first point, any uncertainty in the noise of the first point affects the results of every other point along the line. With the noise figure meter setup, the noise can vary on the order of ±0.004 dB. This uncertainty is represented in Fig. 3(b). The three black curves represent the effect on the measured excess noise at the upper end (+0.004 dB), middle, and lower end (−0.004 dB) of the uncertainty range. A significant change in the measured $F(M)$ is visible.

An approach to circumvent this issue is to use a reference line so that the measured points are independent of each other. This approach is similar to one presented by Bulman *et al*. [14]. The APD is biased at a low voltage (−10 V) to ensure unity gain and unity $F(M)$ and to ensure the device is fully depleted as seen in Fig. 2(b). Then, at this fixed bias, the intensity of incident light is increased, and the noise is measured. This measurement is shown by the black points in Fig. 3(a) and represents only the I_{photo} contribution to the noise. The inset of Fig. 3(a) shows a blown-up plot of this measured line. These points are then fit with a line, and those fit values are used to calculate $F(M)$ from the points in red in Fig. 3(a) using the following equation:

$$F(M) = N_{measured}/(N_{line} M), \tag{4}$$

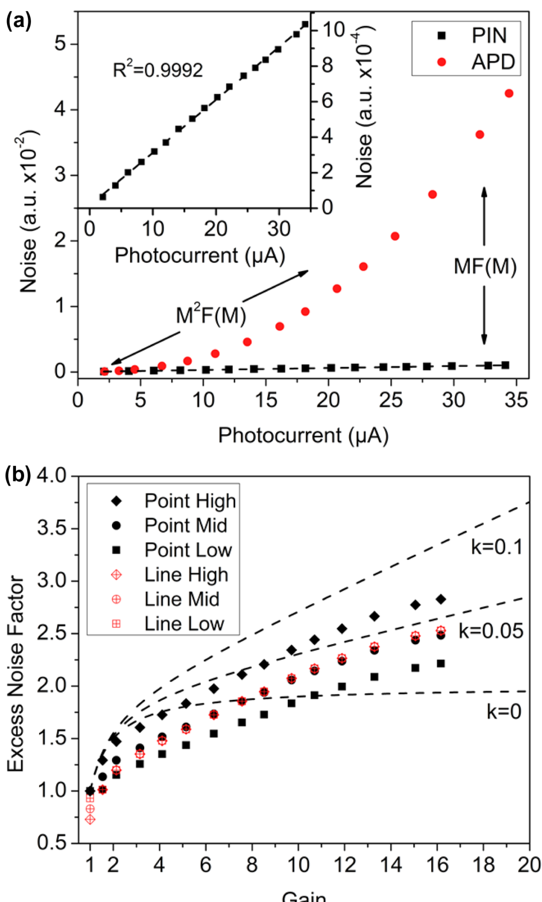

Fig. 3. (a) Measured noise of a 100 μm diameter device under a fixed illumination intensity with increasing bias (APD curve), the measured noise under fixed bias (−10 V) and varying illumination intensity (p-i-n curve), and (inset) a blown-up plot of the p-i-n curve. (b) Excess noise factor from the point method for different first point uncertainties in black, and the excess noise factor from the line method for different first point uncertainties in red.

where $N_{\text{measured}} = 2q I_{\text{photo}} R \Delta f M^2 F(M)$ is the measured noise under higher bias with gain, N_{line} is the noise of the black line at the same photocurrent as the corresponding red point. Note that only M is being divided instead of M^2 since N_{line} already accounts for one factor of M via the increase in photocurrent. The calculated $F(M)$ using this method with the same uncertainty in the first point as with the point method is plotted as the red points in Fig. 3(b). For the red curves as the noise of the first point changes, none of the subsequent points are affected. Therefore, this line reference method offers a more robust $F(M)$ calculation compared to calculating $F(M)$ based solely on the first point.

5. FREQUENCY DEPENDENCE

For "high-frequency" noise measurements above 10 MHz (the lower frequency limit of an Agilent 8973 NFA), an NFA can be used in a configuration shown in Fig. 4(a) in which a bias tee is used to simultaneously provide an isolated DC bias to a device under test (DUT) and couple the AC response to the NFA. Additionally, above 10 MHz, a group from the University of

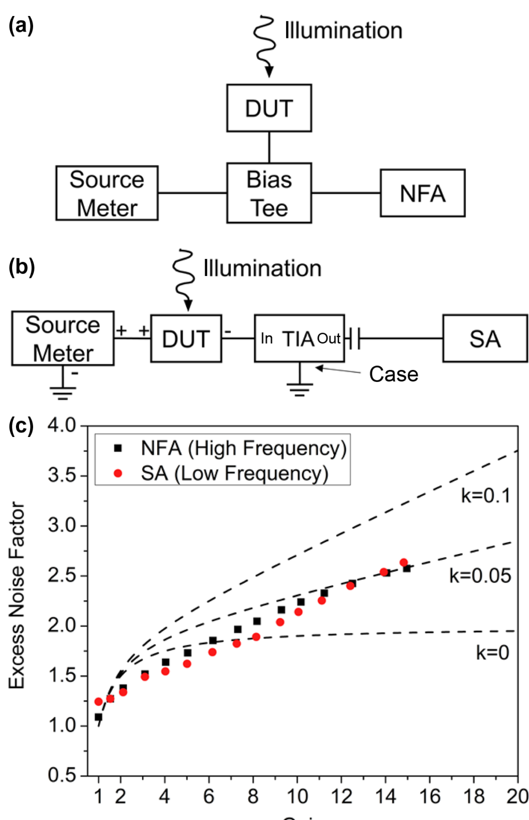

Fig. 4. (a) Noise-figure-analyzer-based setup for measurements above 10 MHz. (b) Spectrum-analyzer-based setup for measurements between ∼20 kHz and ∼400 kHz. (c) Excess noise factor versus gain for the same 100 μm diameter device using the two different setups in (a) and (b).

Sheffield has demonstrated a noise measurement setup using a transimpedance amplifier (TIA) that can provide accurate measurement results for high dark current and high capacitance APDs [15]. However, neither setup is suitable for measuring devices at frequencies under 10 MHz. A setup that can measure below 10 MHz is useful if, for instance, the DUT has a bandwidth less than 10 MHz.

Figure 4(b) shows the schematic for such a setup that can measure the $F(M)$ of a device at as low as ∼20 kHz. In this setup, the DUT is probed with a ground-signal probe with the positive link connected to the input of a Femto DLPCA-200 TIA and the negative link connected to the positive port on a Keithley 2400 SourceMeter. The negative port of the SourceMeter is attached to the metal case of the TIA. The output of the TIA is routed to the input of an Agilent E4440A spectrum analyzer (SA). Since the TIA has a built-in AC couple, a DC bias can be applied across the DUT, and the DC signal is isolated from the SA. The TIA is set to the low-noise performance range with a transimpedance of 10^5 V/A. This gain was chosen to ensure the TIA was not overloaded. The upper limit of measurement frequencies for this setup is ∼400 kHz and is limited by the bandwidth of the TIA. This setup was designed with the help of Leonardo DRS [16].

To confirm the viability of this setup, a 100 μm diameter AlInAsSb APD was measured with the high-frequency NFA-based setup in Fig. 4(a) and the "low-frequency" SA-based setup

in Fig. 4(b). The SA was centered at 68.7 kHz with a resolution bandwidth of 47 Hz. This measurement frequency was selected because the system noise floor was low enough to detect the noise of the DUT and avoid ambient noise sources. The results of these measurements are shown in Fig. 4(c). Aside from the first point, which is prone to increased uncertainty as previously discussed, there is at most an 8% difference between the two measurements.

6. WAVELENGTH DEPENDENCE OF $F(M)$

Another factor to consider when measuring $F(M)$ is the wavelength of light used as different wavelengths can lead to drastically different $F(M)$ measurements. The difference originates from wavelength-dependent absorption, which can lead to different carrier injection profiles. Typically, from the infrared to the visible, the absorption coefficient in a semiconductor material increases as the wavelength decreases. For short wavelengths, such as 445 nm, the light is absorbed very close to the incident surface. In a top-illuminated p-i-n structure, this quick absorption enables pure electron injection into the multiplication region. In many semiconductors, pure electron injection is favorable because the impact ionization coefficient for electrons is greater than that for holes. This, in turn, results in a lower-k factor resulting in lower $F(M)$ at a given gain. For longer wavelengths, such as 633 nm, much of the light is absorbed throughout the multiplication region, resulting in mixed injection with higher-k factors and higher $F(M)$ at a given gain as both electrons and holes are injected into the multiplication region.

Specifically, for the $Al_{0.7}InAsSb$-based APDs studied in this paper, 445 nm (laser diode), 543 nm (He–Ne laser), and 633 nm (He–Ne laser) light was used to measure $F(M)$ under different injection regimes. The approximate thickness x to absorb a fraction η of the incident light (ignoring surface and interface reflections) can be calculated using the following expression:

$$x = -\left(\ln\left(1-\eta\right) + \alpha_{\mathrm{GaSb}} x_{\mathrm{GaSb}}\right) / \alpha_{70\%} + x_{\mathrm{GaSb}}, \tag{5}$$

where $\alpha_{70\%}$ is the absorption coefficient of $Al_{0.7}InAsSb$ at a given wavelength, α_{GaSb} is the absorption coefficient of GaSb at a given wavelength, and x_{GaSb} is the thickness of the GaSb cap layer (30 nm). Using previously published absorption coefficients for $Al_{0.7}InAsSb$ [17] and for GaSb [18], the approximate thickness to absorb 99% of the incident light is 106 nm, 397 nm, and 706 nm for 445 nm, 543 nm, and 633 nm light, respectively. Comparing these lengths to the structure from Fig. 1 shows that 445 nm light should give essentially pure electron injection, whereas, 633 nm light results in a more uniform mixed injection. $F(M)$ was measured for these three wavelengths and is plotted in Fig. 5. It should be noted that the light intensity for the three wavelengths was chosen to ensure that the same photocurrent ~2 μA was measured at −20 V. The light intensities needed were ~202 μW, ~46 μW, and ~21 μW for 445 nm, 543 nm, and 633 nm light, respectively. For these three wavelengths, the k factor ranges from ~0.01 for 445 nm light to ~0.09 for 633 nm light. For the 445 nm curve, $F(M)$ scales below the $k = 0$ curve out to a gain of ~10, a phenomenon commonly seen in Sb-based APDs [1,11,19].

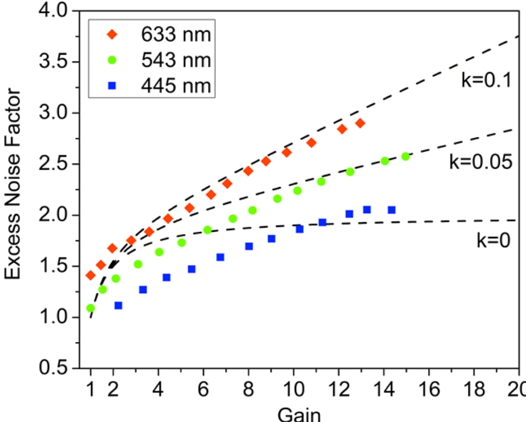

Fig. 5. Excess noise factor versus gain for ~21 μW of 633 nm light, ~46 μW of 543 nm light, and ~202 μW of 445 nm light.

7. GAIN CORRECTIONS

The final consideration with excess noise factor deals with the determination of the gain. The easiest and most straightforward way to calculate gain in an APD is to designate a point in the "flat" region of the I-V as the unity gain point. With this definition, all current values above that unity point are considered gain. In Fig. 2(a), there appears to be a broad flat region in the photocurrent of the I-V after the device has fully depleted from −5 to −25 V. However, when the I-V is plotted on a linear scale and "zoomed in" around the flat region as plotted in Fig. 6(a), there is a slight slope in the photocurrent plot. This small increase in current is attributed to the slight increase in carriers diffusing from the p-contact region into the high-field i region as the depletion width increases into the contact layers under higher bias. It should be noted that the slope of this flat region will increase as the background concentration of the intrinsic region increases and as the doping concentration of the contact layer decreases. Without taking this slight bias-dependent responsivity into account, the gain can be simply calculated by calling the current at −20 V unity and calculating the gain with this reference point. The black curve titled point method is shown in the inset of Fig. 6(a). Using this approach, the highest gain at −46.5 V is ~17.3.

A straightforward method to account for this bias-dependent responsivity is to fit a line to the flat region and define the current along that line as unity. With this method, any current above the line is considered gain. This method was used to fit a line between −10 and −20 V. The result is the "Linear fit" line in Fig. 6(a), and the resulting gain is plotted in the inset. It should be noted that the max gain has been reduced to ~15.9. A more precise way to account for this bias-dependent responsivity is to use a fit presented by Woods *et al.* [20]. The equation is as follows:

$$I = A + B(V + V_D - k_B T/q)^{1/4}, \tag{6}$$

where I is the photocurrent, A and B are fitting constants, V is voltage, k_B is Boltzmann's constant, T is temperature, and q is the elementary charge. V_D is the diffusion voltage expressed as

$$V_D = (k_B T/q)\ln(N_A N_D/n_i^2), \tag{7}$$

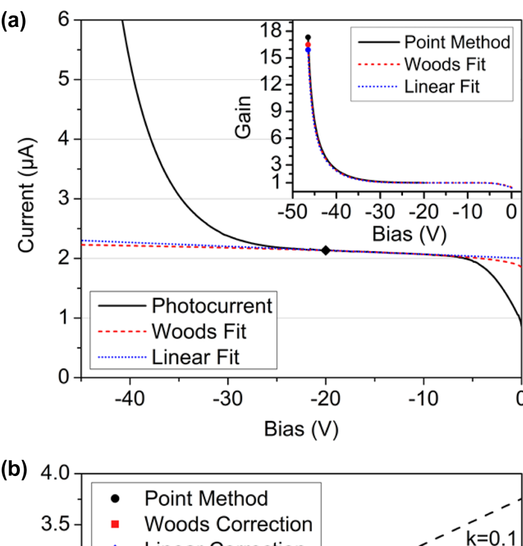

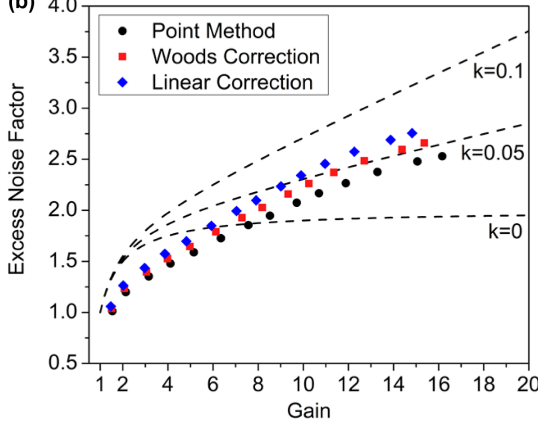

Fig. 6. (a) The photocurrent from Fig. 2(a) plotted on a linear scale with both the Woods fit and Linear fit, and (inset) the resulting gain from a simple point fit, Woods fit, and Linear fit. (b) Excess noise factor versus gain for each of the three gain calculation methods.

where N_A and N_D are the p- and n-contact doping concentrations, respectively, and n_i is the background concentration of the intrinsic region. For this device, N_A and N_D are both 2×10^{18} cm^{-3} and from the inset of Fig. 2(b) n_i is $\sim 5 \times 10^{15}$ cm^{-3}. This method was used to fit a curve between −10 and −20 V. The result is the "Woods fit" line in Fig. 6(a), and the resulting gain, extracted from the current above the fit line, is plotted in the inset. With this fitting approach, the maximum gain was ∼16.5.

Figure 6(b) shows the resulting $F(M)$ when using the point method, the Woods correction, and the linear correction. Using the point method gives the highest gain and the lowest $F(M)$ since here the bias-dependent responsivity is treated as gain. The linear correction gives the lowest gain and highest $F(M)$ as it is a simple fit that attributes some of the gain above −20 V to bias-dependent responsivity. The Woods correction gives both intermediate gain and $F(M)$ and is the preferred choice for calculating gain as the fit accounts for the physical parameters of the structure and better captures the bias-dependent responsivity compared to the linear correction.

8. CONCLUSION

We discussed four factors to consider when measuring the excess noise factor for low-noise APDs. First, we showed that calculating $F(M)$ based on a reference line instead of the first measured point led to a more robust $F(M)$ calculation that was less susceptible to measurement uncertainty. We then presented three potential setups for measuring excess noise that were valid for different frequency ranges. Two setups were for frequencies greater than 10 MHz and have been previously established. A third design for a setup was presented that allows $F(M)$ measurements at frequencies as low as ∼20 kHz. Next, we discussed the effects of illumination wavelength on the measured $F(M)$. Shorter wavelengths provided more pure electron injection into the multiplication region, leading to lower measured $F(M)$. Longer wavelengths provided mixed carrier injection, leading to an increase in the measured $F(M)$. Finally, we presented three methods for calculating the gain in an APD and showed their effects on the measured $F(M)$. These four considerations were important for evaluating excess noise measurements on Sb-based, and more generally, low-k-factor materials.

Funding. Defense Advanced Research Projects Agency (W909MY-12-D-0008, W911NF-17-1-0065); Army Research Office (W911NF-17-1-0065).

Disclosures. The authors declare no conflicts of interest.

Data availability. Data underlying the results presented in this paper are not publicly available at this time but may be obtained from the authors upon reasonable request.

REFERENCES

1. J. C. Campbell, "Evolution of low-noise avalanche photodetectors," IEEE J. Sel. Top. Quantum Electron. **28**, 3800911 (2022).
2. R. J. McIntyre, "Multiplication noise in uniform avalanche diodes," IEEE Trans. Electron Devices **ED-13**, 164–168 (1966).
3. V. M. Robbins, T. Wang, K. F. Brennan, K. Hess, and G. E. Stillman, "Electron and hole impact ionization coefficients in (100) and in (111) Si," J. Appl. Phys. **58**, 4614–4617 (1985).
4. M. E. Woodson, M. Ren, S. J. Maddox, Y. Chen, S. R. Bank, and J. C. Campbell, "Low-noise AlInAsSb avalanche photodiode," Appl. Phys. Lett. **108**, 081102 (2016).
5. S. R. Bank, J. C. Campbell, S. J. Maddox, M. Ren, A.-K. Rockwell, M. E. Woodson, and S. D. March, "Avalanche photodiodes based on the AlInAsSb materials system," IEEE J. Sel. Top. Quantum Electron. **24**, 3800407 (2018).
6. A. H. Jones, S. D. March, S. R. Bank, and J. C. Campbell, "Low-noise high-temperature AlInAsSb/GaSb avalanche photodiodes for 2-µm applications," Nat. Photonics **14**, 559–563 (2020).
7. A. A. Dadey, J. A. McArthur, S. R. Bank, and J. C. Campbell, "Separate absorption, charge, and multiplication avalanche photodiode with a digital alloy Al0.05 In0.95 As0.93 Sb0.07 absorber for mid-IR detection," in *IEEE Photonics Conference (IPC)* (2022), pp. 1–2.
8. S. H. Kodati, S. Lee, B. Guo, A. H. Jones, M. Schwartz, M. Winslow, N. A. Pfiester, C. H. Grein, T. J. Ronningen, J. C. Campbell, and S. Krishna, "AlInAsSb avalanche photodiodes on InP substrates," Appl. Phys. Lett. **118**, 091101 (2021).
9. X. Jin, B. Guo, H. Lewis, S. Lee, B. Liang, S. Krishna, J. C. Campbell, and J. P. R. David, "Excess noise measurements in Al0.85Ga0.15As0.56Sb0.44 avalanche photodiodes," Proc. SPIE **12139**, 59–66 (2022).
10. S. Lee, X. Jin, H. Jung, H. Lewis, Y. Liu, B. Guo, S. H. Kodati, M. Schwartz, C. Grein, T. J. Ronningen, J. P. R. David, J. C. Campbell, and S. Krishna, "High gain, low noise 1550 nm GaAsSb/AlGaAsSb avalanche photodiodes," Optica **10**, 147–154 (2023).
11. J. P. R. David, X. Jin, H. Lewis, B. Guo, S. Lee, H. Jung, S. H. Kodati, B. Liang, S. Krishna, and J. C. Campbell, "Avalanche multiplication and excess noise characteristics in antimony-based avalanche photodiodes," Proc. SPIE **12274**, 54–65 (2022).

12. S. J. Maddox, S. D. March, and S. R. Bank, "Broadly tunable AlInAsSb digital alloys grown on GaSb," Cryst. Growth Des. **16**, 3582–3586 (2016).
13. C. Frisk, Y. Ren, J. Olsson, T. Törndahl, F. Annoni, and C. Platzer-Björkman, "On the extraction of doping concentration from capacitance–voltage: a Cu2ZnSnS4 and ZnS sandwich structure," IEEE J. Photovolt. **7**, 1421–1425 (2017).
14. G. E. Bulman, V. M. Robbins, and G. E. Stillman, "The determination of impact ionization coefficients in (100) gallium arsenide using avalanche noise and photocurrent multiplication measurements," IEEE Trans. Electron Devices **32**, 2454–2466 (1985).
15. J. E. Green, J. P. R. David, and R. C. Tozer, "A transimpedance amplifier for excess noise measurements of high junction capacitance avalanche photodiodes," Meas. Sci. Technol. **23**, 125901 (2012).
16. R. Scritchfield and P. Mitra, and Electro-optical & Infrared Systems, Leonardo DRS, 13532 North Central Expressway, Dallas, Texas 75243 (personal communication, 2022).
17. Y. Yuan, J. Zheng, A. K. Rockwell, S. D. March, S. R. Bank, and J. C. Campbell, "AlInAsSb impact ionization coefficients," IEEE Photon. Technol. Lett. **31**, 315–318 (2019).
18. D. E. Aspnes and A. A. Studna, "Dielectric functions and optical parameters of Si, Ge, GaP, GaAs, GaSb, InP, InAs, and InSb from 1.5 to 6.0 eV," Phys. Rev. B **27**, 985–1009 (1983).
19. J. Taylor-Mew, V. Shulyak, B. White, C. H. Tan, and J. S. Ng, "Low excess noise of Al0.85Ga0.15As0.56Sb0.44 avalanche photodiode from pure electron injection," IEEE Photon. Technol. Lett. **33**, 1155–1158 (2021).
20. M. H. Woods, W. C. Johnson, and M. A. Lampert, "Use of a Schottky barrier to measure impact ionization coefficients in semiconductors," Solid-State Electron. **16**, 381–394 (1973).

128.62.161.113 {ts '2023-05-31 13:33:11'}